Fatigue Behaviour of Thermal Cutted Steel Structural Element

J. Kramberger[1], N. Jezernik[1] and S. Glodež[2]

[1] University of Maribor, Faculty of Mechanical Engineering, Smetanova 17, SI-2000 Maribor, Slovenia
[2] University of Maribor, Faculty of Natural Science and Mathematics, Koroška c. 160, SI-2000 Maribor, Slovenia

ABSTRACT. *This paper presents an investigation the effects of thermal cutting process on the fatigue life of selected structural elements. Thermal cutting process introduces a roughened surface on the cut edge and also changes in micro-structural properties of material in heat affected zone. A multi scale numerical approach for evaluation of crack initiation and propagation is presented. Crack initiation is dealt on micro scale model, while taking into account the effects of micro structural and geometrical changes at the cut edges of selected structural element. Residual stresses induced by the thermal loading are neglected. Individual grains of synthetic microstructure are simulated using Voronoi tessellation. Micro-crack initiation mechanism was based on Tanaka-Mura model. Some improvements were added to this model. Crack propagation is then solved on a macro scale model using linear elastic fracture mechanics approach. Some experimental testing was also performed so that the accuracy of the numerical model was checked. The results of proposed computational model show a reasonable correlation with experimental results.*

INTRODUCTION

Thermal cutting process itself causes a significant roughness on the cut edge and also changes microstructural properties of material in heat affected zone (HAZ). Surface topography, which is usually represented by roughness parameters, such as average roughness height R_a, decreases fatigue life as it causes more stress concentrations and hastens crack initiation. Heat input of particular cutting process causes hardening and softening in HAZ and creation of internal residual stresses. This also has an effect of fatigue life, that may be detrimental or beneficial.

The behaviour of micro-cracks under fatigue loading differs substantially from the behaviour of long-cracks [1, 2]. Existing research in micro-crack nucleation has shown for many materials that micro-cracks are initiated on slip bands of grains and stretch across whole grain [3]. The often proposed method to solve this problem, is by using Tanaka-Mura model for micro-crack initiation [4].

Using this model, the number of stress cycles N_c required for the micro-crack initiation can be determined as follows:

$$N_c = \frac{8GW_s}{\pi(1-\nu)d\left(\Delta\tau_s - 2\mathrm{k}\right)^2} \tag{1}$$

Eq. 1 presumes that micro-cracks form along the slip band of grains, depending on slip band length d and average shear stress range on the slip band $\Delta\tau_s$. Other material constants like shear modulus G, specific fracture energy per unit area W_s, Poisson's ratio ν, and frictional stress of dislocation on the slip plane k can be found in the specialised literature. Data for structure (marthensite) dealt in this paper can be found in reference [5].

Tanaka-Mura model still has two deficiencies that limit its usage. Model deal only with micro-crack nucleation in separate grains and does not deal with macro-crack coalescence from existing micro-cracks. Another problem is that this model uses an average shear stress to determinate micro-crack nucleation. In our previous investigation to simulate micro-crack initiation [6], it often happened that an existing micro-crack significantly raised stresses of neighbouring grain, yet the average shear stress in this grain was still below the threshold needed for micro-crack nucleation, therefore no nucleation occurred. This problem becomes increasingly pronounced when using lower load level, that is in high cycle fatigue regime. The aim of this study is to present a few improvement to the Tanaka-Mura model to focuse on solving mentioned problems.

NUMERICAL MODELLING

In order to simulate both the problem of crack initiation as well as long crack propagation, a multi-scale model was created. Numerical analysis was split into two parts: microscopic - for assessment of crack initiation and macroscopic - for assessment of crack propagation [7]. Fig. 1 shows both models (macro and micro) that were created in this manner. Macro model represents a full scale model of a structural element subjected to selected load level. Micro model was created in the place where the highest stress concentration (at the hole) and formation of cracks are expected. Stress distribution in macro-model is applied to the boundary edges of micro-model (top, right, and bottom edge).

Numerical simulation of crack-initiation was performed with ABAQUS [8], using a plug-in that was written specially for handling micro-crack nucleation and coalescence. Used model needs to simulate the material properties of hardened marthensitic layer as well as a surface roughness of cut edge [9]. With respect to the micro-hardness measurements [10], the size of model was chosen to be equal 0.3×0.3 mm. Cut edge roughness was simulated with a Bezier spline, that has an amplitude and period similar to maximal measured roughness. Individual grains are simulated with randomly

generated Voronoi tessellation and were given randomly oriented [11, 12] orthotropic material properties of marthensite ($C_{11} = C_{22} = C_{33} = 233$ GPa, $C_{12} = C_{13} = C_{23} = 135$ GPa, $C_{44} = C_{55} = C_{66} = 118$ GPa [5]).

Considering the average grain size of 20 μm the whole model consists of appropriately 300 individual grains. The right image in Fig. 1 shows such a model, with slip bands drawn through centres of grains. The surrounding grains (with no slip bands indicated), serve as a buffer zone to minimize the numerical mismatch at boundaries (top, right and bottom edge on the right image of Fig. 1) and do not partake in micro-crack evaluation.

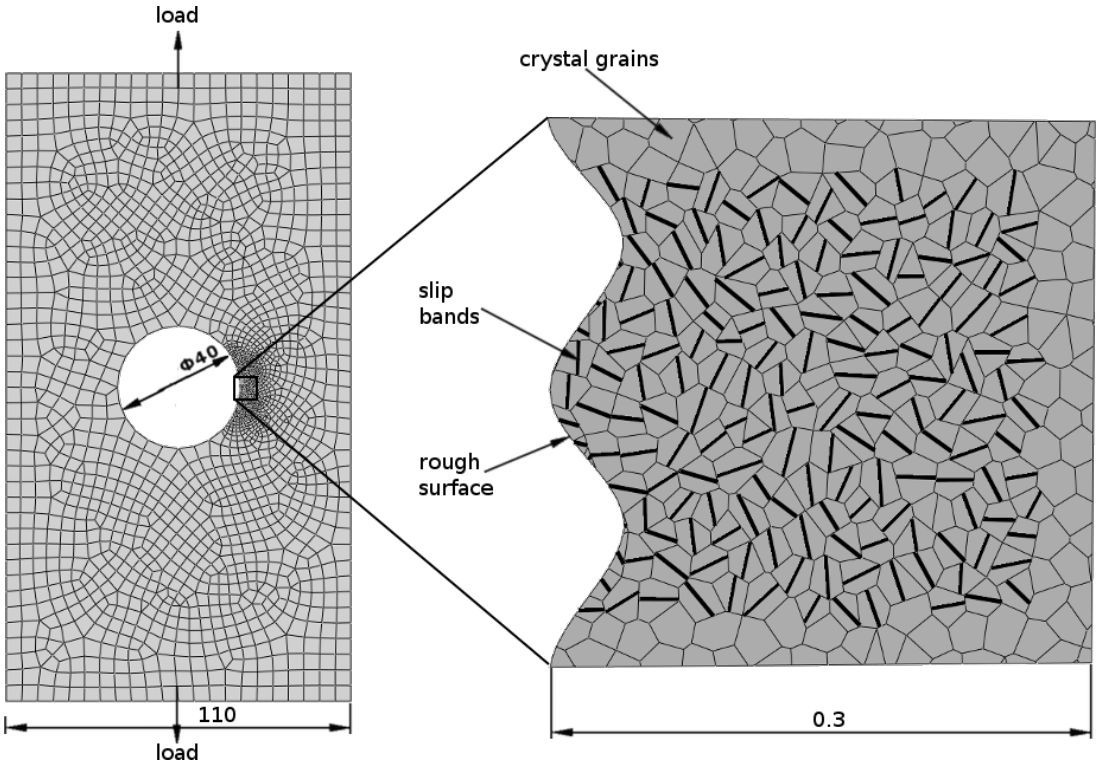

Figure 1. Macro and micro model.

Multiple slip bands

When simulating crack nucleation in particular grain, multiple slip bands were evaluated. For each grain there was one slip band created through the centre of the grain and additional slip bands were created with a 2 μm offset from the first, as is shown in Fig. 2.

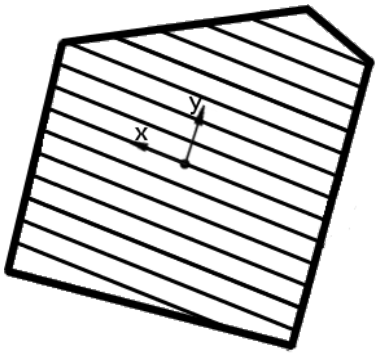

Figure 2. A grain with multiple slip bands.

Fig. 3 shows a case where the first micro-crack was nucleated in the left grain and influenced its neighbouring grain on the right, so that a micro-crack in it nucleated far from the centre (black dot represent centres of grains), close to the first micro-crack. The proximity of nucleated micro-cracks also enables easier micro-crack coalescence than in a model where micro-cracks are allowed to go through grain centres only [5, 10].

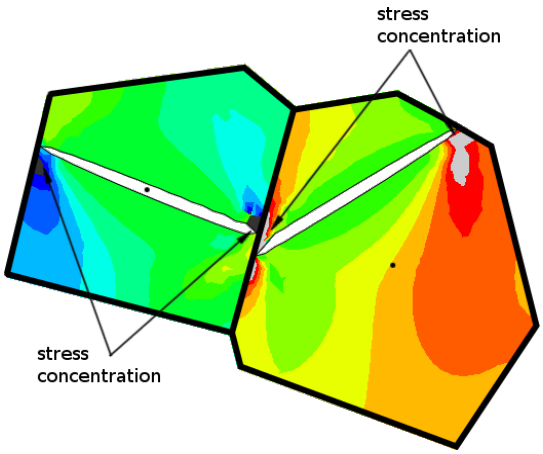

Figure 3. Example of nucleated cracks along slip lines.

Crack coalescence

A conservative approach was taken to enable crack coalescence. Whenever a new micro-crack was introduced in the model, all possible combination of micro-cracks were analysed to see if the average stress on a straight line between two micro-cracks surpasses yield stress of the material. If this was the case, a seam was created on this line, effectively transforming two micro-cracks into a single crack (Fig. 4).

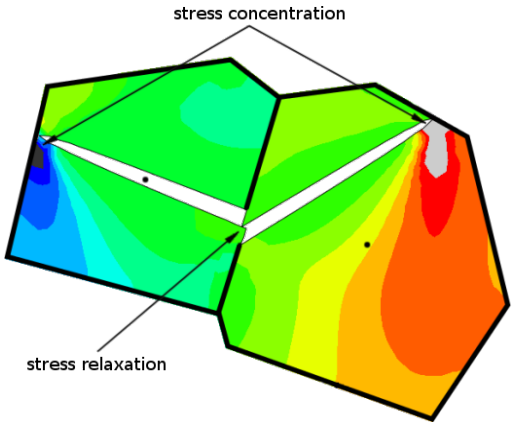

Figure 4. Example of two micro-cracks coalescing.

Note significant stress relaxation in Fig. 4 with respect to Fig. 3. When calculating cycles required for crack initiation, no cycles were attributed to crack coalescences (it is simulated as being instantaneous), so the total cycles of crack initiation equal the sum of cycles needed for each micro-crack to nucleate.

Segmented micro-cracks

In Fig.5 is shown shear stress distribution along slip band for different stages of initial crack evolution. Fig. 5a shows shear stress range (black solid line) along a slip band of a grain, which neighbouring grain already has a micro-crack. This causes a significant stress concentration on the side of the slip band that is adjacent to the existing micro-crack.

Using Tanaka-Mura model would not cause a micro-crack to nucleate in this case, as average shear stress range (gray dotted line) is lower than the required threshold (gray solid line). This problem was solved using segmented micro-cracks. Figures 5b, 5c, and 5d show the evolution of micro-crack nucleation using four segments along the slip band. Fig. 5a shows that the stress level on the leftmost segment (black dotted line) surpasses the threshold stress range and a micro-crack can occur there. Fig. 5b shows next iteration where a seam was created on the first segment causing stress relaxation there and a stress increases on the second segment so that the stress range surpasses the threshold. Figures 5c and 5d show the next two iterations where a micro-crack seam progresses through third and fourth segment and finally forms along the whole slip band.

Since proposed algorithm for crack initiation goes through multiple iterations, it is necessary to account for dislocation pile-up by keeping track of the damage that was accumulated over previous stages.

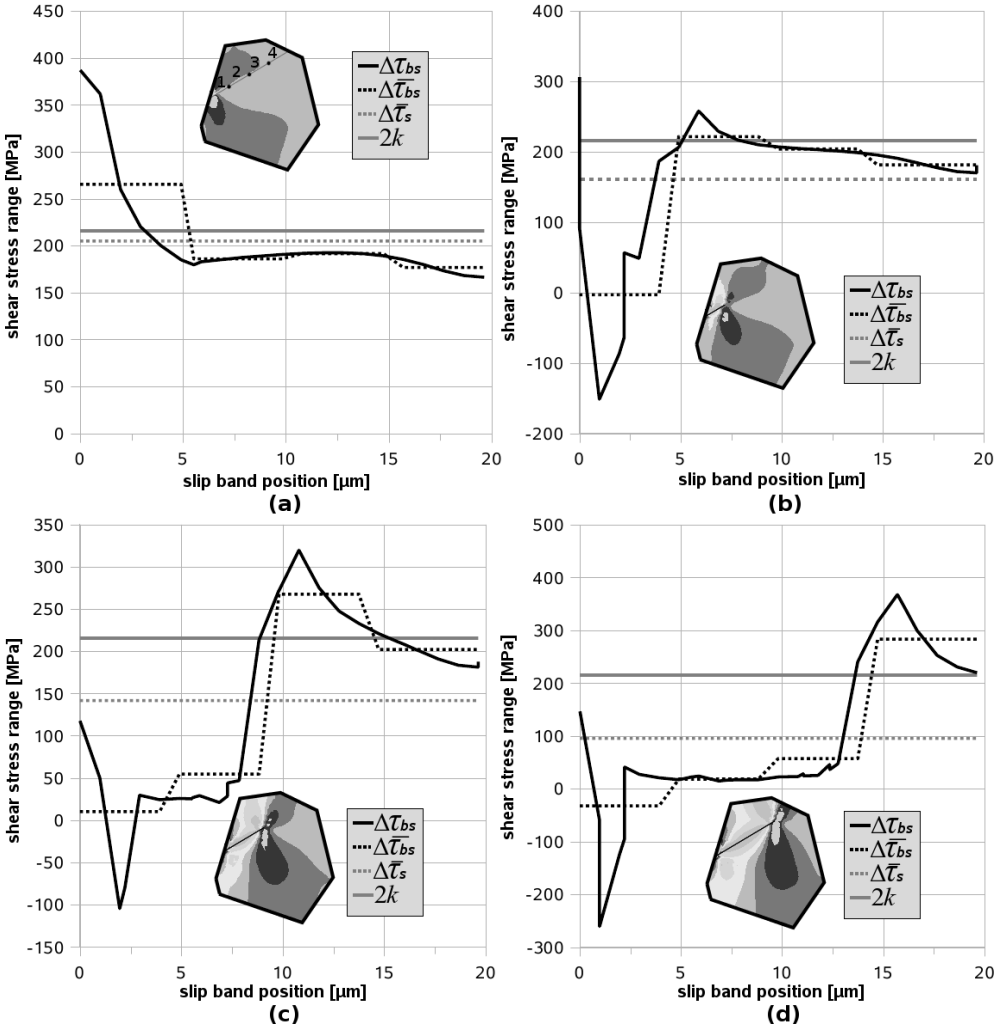

Figure 5. Shear stress distribution along slip band.

In the beginning, total damage needed for micro-crack nucleation is calculated for slip bands of every grain, using following equation:

$$TD_b = \frac{8\,GW_s}{\pi(1-\nu)d_b} \tag{2}$$

where TD_b represents a total amount of damage that is required for micro-crack nucleation on a particular slip band (index b), where d_b is the length of particular slip band.

Then in each stage partial damage for each segment of each slip band is calculated:

$$PD_{bs} = \left(\Delta\overline{\tau} - 2\mathrm{k}\right)^2 \tag{3}$$

where $\Delta_{bs}\tau$ and PD_{bs} represent average shear stress range and amount of damage that is accumulated in one loading cycle on a segment *s* of slip band *b*.

The number of cycles N_{bs}, required for micro-crack nucleation on each segment, is calculated with the following equation:

$$N_{bs} = \frac{\frac{TD_b}{n_s} - AD_{bs,i}}{PD_{bs}} \tag{4}$$

where $AD_{bs,i}$ represents already accumulated damage in each segment of stage *i* and n_s is the number of segments per slip band.

Then a seam is created on the segment with the smallest N_{bs} and the accumulated damage for next stage $AD_{bs,stage+1}$ increased.

$$AD_{bs,stage+1} = AD_{bs,stage} + PD_{bs} \cdot N_{bs,min} \tag{5}$$

Model with a new seam is then recalculated and used for next iteration where the whole process is repeated.

In the beginning seams tend to occur scattered around the model and form preferably in larger grains that are favourably oriented and have higher shear stresses. But after a while existing micro-cracks start coalescing, causing local stress concentrations and amplifying the likelihood of new micro-cracks forming near already coalesced crack. When this crack grows to sufficient length, crack initiation is considered to be finished. The resulting macro-cracks was used as an initial crack for crack propagation. The sum of $N_{bs,min}$ for all stages represent total crack initiation cycles N_i.

$$N_i = \sum_{stage=1}^{n} N_{bs,min} \tag{6}$$

Crack propagation

In order to asses total lifetime, crack propagation of a long crack also have to be calculated. The length and the direction of initial crack were selected, so that they resemble the coalesced micro-cracks obtained in crack initiation stage. This crack was then propagated through macro-model according to the linear elastic fracture mechanics (LEFM). Crack propagation cycles were calculated using the Paris law:

$$\frac{da}{dN_p} = C\left[\Delta K(a)\right]^m \tag{7}$$

with crack growth parameters $C = 6 \cdot 10^{-9}$ (units: MPa, m) and $m = 3$, which are taken for treated material from literature [13].

Stress intensity factor range ΔK and angle of crack propagation were both calculated with ABAQUS [8]. As a criterium of crack propagation direction, maximum tangential stress (MTS) method was used. Fig. 6 shows the relationship between crack length and stress intensity factor range. Results for crack initiation, propagation and total life-time are presented in Table 2.

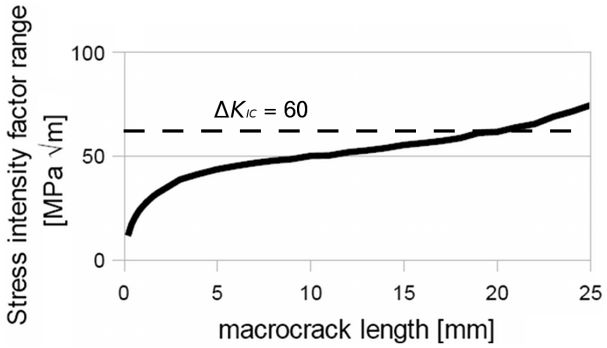

Figure 6. Stress intensity factor range with respect to crack length.

EXPERIMENTAL TESTING

In this study investigated steel S960QL (WELDOX 960E) is often used in heavy-lifting industries and is subjected to dynamically loaded environment with high number of required loading cycles. Since components used in this cases are usually thermally cut (with laser for thinner and plasma for thicker components) and built-in without any additional surface treatment, microstructural properties [13, 14] and surface roughness [15, 16] were also incorporated in the simulation. Fatigue testing was performed on nine laser cut specimens. Specimen dimensions were equal 200 mm × 110 mm × 5 mm (Fig. 7), with a circular hole of 40 mm, that creates a stress concentration factor $K_t = 2.28$.

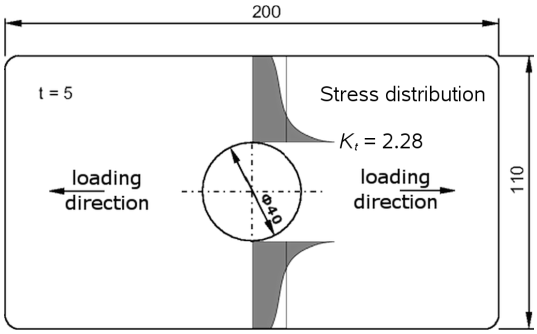

Figure 7. Test specimen.

According to the performed static tensile test, the yield stress of material was $R_{p0,2} = 1026$ MPa and the ultimate tensile stress $R_m = 1064$ MPa, with 15% elongation at

breakage. Table 1 shows the chemical composition of investigated material. Basic material parameters of marthensitic layer, required for Tanaka-Mura model, were taken from literature [5]: shear modulus $G = 118$ GPa, specific fracture energy per unit area $W_s = 2.0$ kJ/m^2, Poisson's ratio $\upsilon = 0.3$, and frictional stress of dislocation on the slip plane $k = 108$ MPa.

Table 1. Chemical composition of steel S960QL

C	Si	Mn	P	S	Cr	Ni	Mo	V	Ti	Cu	Al	Nb	B	N
0.17	0.21	1.24	.008	.002	0.19	0.05	.586	.043	.002	0.01	.057	.014	.001	.005

Cut edge properties

Surface roughness of cut edge was determined using a perthometer. Since the expected roughness was in range $5<R_a<10$ μm, a reference measurement length was chosen to be equal 12.5 mm. Average arithmetic roughness height was found to be $R_a = 5.0$ μm and maximal roughness height was $R_z = 37.6$ μm. In simulation, the maximal roughness was modelled, as it can be expected that micro-cracks will likely form where the highest stress concentration exists.

Microstructure

Microstructural analysis was performed to determine the type of microstructure in heat affected zone (HAZ) and its thickness. With scanning electron microscopy (SEM) it was determined that the average grain size in HAZ is 20 μm and the typical distance between marthensitic laths is 2 μm. Fig. 8 shows electron microscope image of investigated material, with some distinct grains shaded for better visualization. Investigated steel is thermo-mechanically treated and tempered so as to produce very fine grained microstructure.

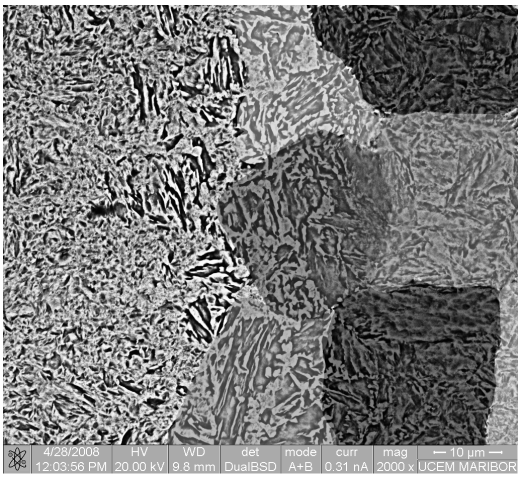

Figure 8. Electron microscope image of investigated steel.

Testing procedure

Fatigue tests were carried out on a pulsating machine Amsler with uni-axial loading and load control. The stress ratio was R = 0.1 with a constant stress amplitude. The used frequency of loading was approximately 150 Hz. Specimens were tested in the same state as they were produced and no additional treatment was performed. Nine specimens were loaded at different stress levels with maximal stress ranging from 460 to 590 MPa. Stress loads were chosen so as to evaluate high cycle fatigue range from $2 \cdot 10^5$ to $2 \cdot 10^6$ cycles.

COMPARISON OF NUMERICAL AND EXPERIMENTAL RESULTS

Fig. 9 shows the comparison of numerical and experimental results. Best fit S-N curve is also included in diagram. Since only one test was carried out at each load level, we were not able to statistically evaluate the data and assess its probability. Nevertheless, exponent of fatigue strength b=-0,087 has been calculated, while assuming that the coefficient of fatigue strength is equal for each specimen.

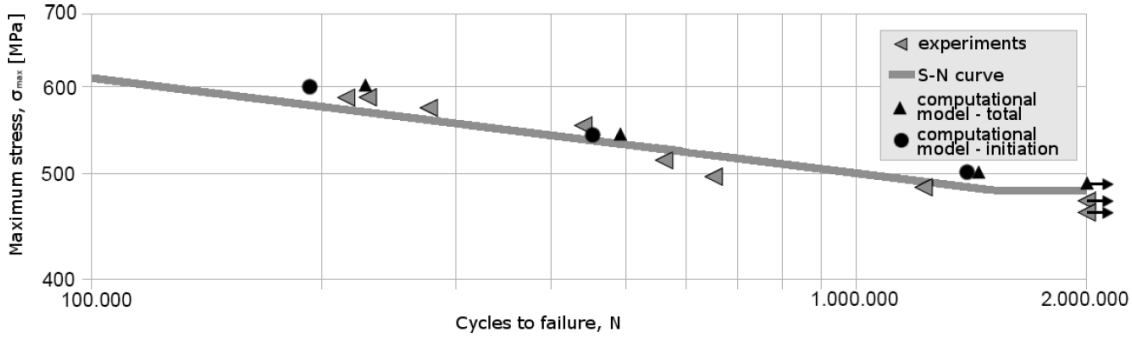

Figure 9. Numerical and experimental results.

The computational results presented in Fig. 9, consist of combined crack initiation and crack propagation part, as shown in Table 2.

Table 2. Initiation and propagation cycles for different load levels

Load level [MPa]	600	550	500	485
Cycles to initiation	194 000	447 000	1 400 000	∞
Propagation cycles	34 000	41 000	47 000	/
Total cycles	228 000	488 000	1 447 000	∞

Numerical simulation was performed on four stress levels: 600, 550, 500, and 485 MPa. Fig. 10 shows a few stages of micro-crack evolution for load level 600 MPa. It is

evident that in the beginning micro-cracks form near the stress concentration due to surface roughness and where grain orientation is 45° with respect to load, so that maximal shear stresses occur. After a while new micro-cracks nucleate near the existing micro-cracks and start coalescing into a larger macro-crack. When macro-crack reached length 0.2 – 0.3 mm simulation was stopped.

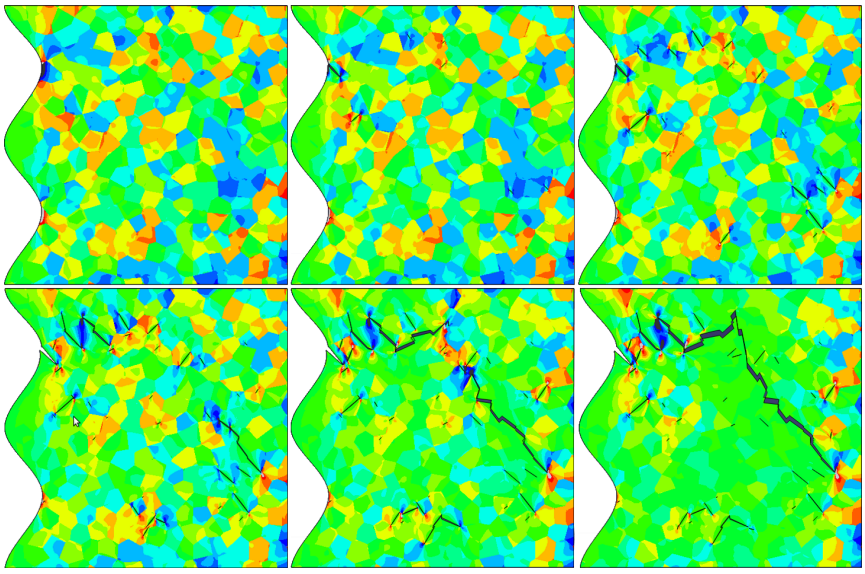

Figure 10. Micro-crack evaluation for load level 600 MPa (left to right).

Fig. 11 shows shear stress distribution and nucleated micro-cracks for load level 485 MPa after $5 \cdot 10^6$ cycles.

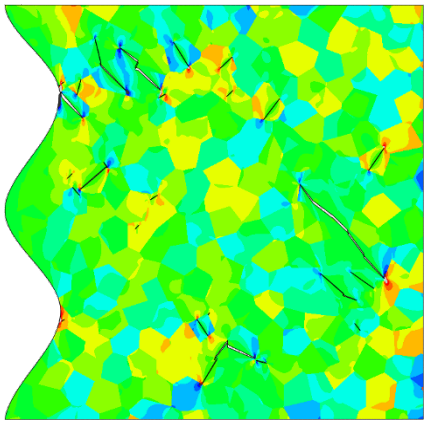

Figure 11.Micro-crack evaluation for load level 485 Mpa after$5 \cdot 10^6$ cycles .

Since no significant crack coalescence occurred it was concluded that crack initiation can not be completed and that the load level is below fatigue limit.

CONCLUSIONS

Fatigue strengths after thermal cutting were numerically and experimentally determined. Crack initiation becomes increasingly important in high cycle fatigue (HCF), as it can amount to more than 90% of components life-cycles. Initiation assessment is also very problematic as it is highly dependent on the minute features, like the microstructure and surface roughness. Using Tanaka-Mura approach to solving crack initiation still leaves open the problem of micro-crack coalescence. Also, it does not handle the problem of significant stress gradients caused by existing micro-cracks as it uses average stress along slip band. The paper presents a possible solution to this problem, by introducing segmented slip bands, where micro-cracks nucleate in multiple stages. Crack coalescence is solved by connecting two micro-cracks, if stresses between them surpass yield stress of material. A plug-in for ABAQUS package was created to handle these features.

The proposed method shows a quite good correlation with experimental testing, but still has some deficiencies. Crack coalescence is solved very conservatively and some method should be applied to evaluate the number of cycles needed for a crack to extend along grain boundary. In the future model other effects like residual stresses should be also considered.

REFERENCES

1. Miller, K.J. (1987) *Fatigue Fract. Eng. Mater. Struct.* **10**, 75–113.
2. Tokaji, K., Ogawa, T., Harada, Y. and Ando, Z. (1986) *Fatigue Fract. Eng. Mater. Struct.* **9**, 1-14.
3. Tryon, R.G., Cruse ,T.A. (1998) *Fatigue Fract. Eng.Mater. Struct.* **21**, 257-267.
4. Tanaka, K. and Mura, T., (1981) *J. Appl. Mech.* **48**, 97-103.
5. Brückner-Foit, A., Huang, X. (2006), *Int. J. Fatigue* **28**, 963-971.
6. Jezernik, N., Glodež, S., Kramberger, J. (2008). In: *CADAM 2008 Proceedings*, 25-26.
7. Taylor, D. (2002) *Comput. Mat. Sci.* **25**, 228-236.
8. Abaqus 6.7 Theory Manual, http://hpce.iitm.ac.in/Manuals/Abaqus_6.7EF1/Documentation/docs/v6.7ef/.
9. Meyer, S., Brückner-Foit, A., Möslang, A. (2003) *Comput. Mat. Sci.* **26**, 102-110.
10. Jezernik, N., Glodež, S., Kramberger, J. (2008). In: *ECF17 Book of Abstracts & Proceedings*, Pokluda, J. (Ed.), Vutium, Brno.
11. Andersson, J. (2005) *Int. J. Fatigue* **27**, 847–852.
12. Simonovski, I., Cizelj, L. (2007) *Int. J. Fatigue* **29**, 2005–2014.
13. Rodopoulos, C. A., Rios, E. R. (2002) *Int. J. Fatigue* **24**, 719-724.
14. Lankford, J. (1985) *Fatigue Eng. Mater. Struct.* **8**, 161-175.
15. Yue, Z. F. (2005) *Engng. Fract. Mechanics.* **72**, 749-757.
16. Antunes, F. V., Ramalho, A., Ferreira, J. M. (2000) *Int. J. Fatigue* **22**, 781-788.